Hierarchically structured meso-macroporous aluminosilicates with high tetrahedral aluminium content in acid catalysed esterification of fatty acids

Arnaud Lemaire [a,1], Quan-Yi Wang [a,b,d,1], Yingxu Wei [b], Zhongmin Liu [b,*], Bao-Lian Su [a,c,*]

[a] Laboratory of Inorganic Materials Chemistry (CMI), University of Namur (FUNDP), 61 rue de Bruxelles, B-5000 Namur, Belgium
[b] Dalian Institute of Chemical Physics, Chinese Academy of Science, 457 Zhongshan Road, 116023 Dalian, China
[c] State Key Laboratory of Advanced Technology for Materials Synthesis and Processing, Wuhan University of Technology, 122 Luoshi Road, 430070 Wuhan, Hubei, China
[d] Graduate School of Chinese Academy of Sciences, 100049 Beijing, China

ABSTRACT

A simple synthesis pathway has been developed for the design of hierarchically structured spongy or spherical voids assembled meso-macroporous aluminosilicates with high tetrahedral aluminium content on the basis of the aqueous polymerisation of new stabilized alkoxy-bridged single molecular precursors. The intimate mixing of an aluminosilicate ester (sec-BuO)$_2$–Al–O–Si(OEt)$_3$ and a silica co-reactant (tetramethoxysilane, TMOS) with variable ratios and the use of alkaline solutions (pH 13.0 and 13.5) improve significantly the heterocondensation rates between the highly reactive aluminium alkoxide part of the single precursor and added silica co-reactant, leading to aluminosilicate materials with high intra-framework aluminium content and low Si/Al ratios. The spherically-shaped meso-macroporosity was spontaneously generated by the release of high amount of liquid by-products (water/alcohol molecules) produced during the rapid hydrolysis and condensation processes of this double alkoxide and the TMOS co-reactant. It has been observed that both pH value and Al–Si/TMOS molar ratio can strongly affect the macroporous structure formation. Increasing pH value, even slightly from 13 to 13.5, can significantly favour the incorporation of Al atoms in tetrahedral position of the framework. After the total ionic exchange of Na$^+$ compensating cations, catalytic tests of obtained materials were realised in the esterification reaction of high free fatty acid (FFA) oils, showing their higher catalytic activity compared to commercial Bentonite clay, and their potential applications as catalyst supports in acid catalysed reactions.

© 2011 Elsevier Inc. All rights reserved.

1. Introduction

Recent studies highlight the promising superiority of hierarchical meso-macrostructured materials in large series of catalytic reactions [1–11], thanks to improved diffusion and mass transfer properties as well as limitation of poisoning and coking, especially when large molecules are used and reactions are performed in viscous liquid phase [12,13]. A large panel of original strategies, often quite tedious to achieve, have been developed to allow the incorporation of desirable porosities at different length scales into one single body. These strategies can be summarised into two categories. One concerns the use of templates such as polymeric beads and silica opals [14–16], soft sacrificial template [17], foam [18,19], emulsions [20,21], ice crystals [22], natural structures [23] such as bacterial threads [24] with the combination of amphiphilic molecules or zeolite crystal seeds [25–28]. Other one is related to post-synthesis treatments [29]. Lately, a self-formation phenomenon of porous hierarchy has been discovered [30–48]. This new strategy is based on the very fast polymerisation of metal alkoxides in aqueous solution, yielding hierarchical meso-macroporous oxide and metallosilicate materials. The macrostructure consists of typically well organised parallel macrochannels of funnel like shape whereas mesoporosity results from the aggregation of inorganic nanoparticles. This strategy has been extended to metal alkyls as precursor [49].

Aluminosilicate composition is heavily involved in catalytic reactions and separation processes [50,51]. Its chemical activity arises from the insertion of trivalent aluminium atoms into a tetrahedral silicate framework, implying charge deficiencies and compensating cations. This creates Lewis and Brönsted acid–base sites which are catalytically active for cracking, isomerisation or alkylation reactions. Synthesised porous aluminosilicate materials with low Si/Al ratios are rare [52] and the preparations from two separated precursors, an aluminium alkoxide and an alkoxysilane, results in hierarchical meso-macroporous aluminosilicates that are

---

* Corresponding authors. Addresses: Laboratory of Inorganic Materials Chemistry (CMI), University of Namur (FUNDP), 61 rue de Bruxelles, B-5000 Namur, Belgium (B.-L. Su), Dalian Institute of Chemical Physics, Chinese Academy of Science, 457 Zhongshan Road, 116023 Dalian, China (Z. Liu).
   E-mail addresses: zml@dicp.ac.cn (Z. Liu), bao-lian.su@fundp.ac.be, baoliansu@whut.edu.cn (B.-L. Su).
   [1] These authors contribute equally to this work.

chemically heterogeneous due to their construction from binary oxides [53–55]. In fact, aluminium alkoxides polymerise faster than alkoxysilanes, forming octahedrally co-ordinated extra-framework aluminium species that may exist in separated bulk, inducing the important loss of selectivity. The synthesis of porous aluminosilicate materials with high aluminium content and a molecular and a homogeneous distribution of the Si–O–Al linkages in the final frameworks still remains a great challenge.

One promising strategy relies on the use of single molecular precursors [56–59]. These molecules, constructed from a pre-formed M–O–Si linkages, are able, under controlled hydrolysis and condensation reactions, to form unequalled chemically homogeneous metallosilicate materials. An Al–Si ester type precursor which already contains an Al–O–Si linkage, the di-*sec*-but-oxyaluminoxytriethoxysilane (*sec*-BuO)$_2$Al–O–Si(OEt)$_3$ has been used in pioneer works [60–63]. More importantly, this single-source molecular precursor possesses, in addition to the preformed Al–O–Si bond, two alkoxide functionalities that are able to undergo fast hydrolysis and polycondensation reactions, rendering possible the auto-generation of a hierarchical meso-macroporosity with unmatched chemical homogeneity, thus, introducing unprecedented acid–base properties with a totally controlled stoichiometry and improved diffusion properties. Previous works have revealed that the Al–O–Si linkage rupture prevention of the single molecular precursor in aqueous solution requires the use of some aluminium selective chelating agents [64] or silica co-reactants such as TMOS, TEOS, TPOS and TBOS [65] in highly alkaline medias. High alkaline condition favours the conversion of aluminium precursors into monomeric tetrahedral O–Al[OH]$_3^-$ species, which is known to preferentially co-polymerise with the silicate anions to form an Al–O–Si network [66–68].

In this work, in order to synthesise a panel of materials with finely tuned Si/Al ratios (1 < Si/Al < 2) without the rupture of the Al–O–Si linkage, tetramethoxysilane (TMOS) as a silica co-reactant in reduced amount were mixed with the di-*sec*-butoxyaluminoxytriethoxysilane due to its high efficiency to favour co-polymerisation between highly reactive aluminium functionalities and the silicon functionalities from the Al–Si ester and TMOS co-reactant [69]. The influence of the (*sec*-BuO)$_2$Al–O–Si(OEt)$_3$/TMOS ratio on the macroporous morphology, textural properties, and aluminium incorporation were studied. The obtained aluminosilicate materials were ion exchanged to obtain acidic form of aluminosilicate materials. Newly synthesised acid-type aluminosilicate materials were then used in acidic catalytic transesterification reactions of a palmitic acid/oleic acid mixture with ethanol to assess their performance [70,71]. Their catalytic behaviour was compared with commercial Bentonite clay, which is a well known FCC catalyst support. These results indicate that a new generation of more efficient catalyst supports has been prepared from the promising single-source molecular precursor route.

2. Experimental

2.1. Preparation of meso-macroporous materials

The Al–Si ester, di-*s*-butoxyaluminoxytriethoxysilane ((Bu^{s}O)$_2$Al–O–Si(OEt)$_3$), was purchased from Gelest, and other chemicals from Aldrich. They were used without any further purification. Aqueous alkaline solutions (pH = 13.0 and 13.5) were prepared by dissolving NaOH in 60 mL of bidistilled water (at a pH of 6.5). Subsequently, 5.0 g of the Al–Si ester were intimately mixed with tetramethoxysilane (TMOS) (molar ratios Al–Si ester/TMOS = 1/1, 2/1 and 4/1) under vigorous stirring (700 rpm) and inert N$_2$ atmosphere for 5 min, resulting into the formation of unique

transparent aluminosilicate phase, made by new stabilized alkoxy-bridged single molecular precursors. This mixture was slowly added dropwise into the NaOH solution under very mild stirring (<100 rpm). After 1 h the mixture was transferred into a Teflon-lined autoclave and heated to 80 °C for 24 h. The solid product was filtered, washed with water, and dried in an oven at 40 °C. Materials are labelled as Al–Si-TM. The number following immediately Al–Si-TM prefixes indicates the pH value used for the synthesis and the following number after the dash (–) represents the ratio of single precursor/silica co-reactant (TMOS). Informations are compiled in Table 1.

Reference materials, prepared without TMOS silica co-reactant at ph 13.0 and 13.5 are named Al–Si-13 and Al–Si-13.5 respectively.

Catalytic tests were achieved by using H$^+$ form of aluminosilicate materials obtained by successive ionic exchange. The ion exchange was made by nine consecutive ion exchange procedures by the immersion of the Al–Si-TM13-1 sample in 0.12 M NH$_4$NO$_3$ ethanol solutions at 80 °C during 1 h.

2.2. Characterisation

Transmission electronic microscopy (TEM) experiments were performed on a Philips TECNAI-10 microscope at an acceleration voltage of 80 kV with sample powders embedded in an epoxy resin and sectioned with an ultramicrotome. The N$_2$ adsorption and desorption isotherms were measured at −196 °C with a volumetric adsorption analyzer, Micromeritics Tristar 3000. The morphology as well as the macroporous array was studied using a Philips XL-20 scanning electron microscope (SEM) and a JEOL JSM 7500 field emission scanning electron microscope (FE-SEM) with conventional sample preparation and imaging techniques. The environments of the Al and Si atoms were studied via ^{27}Al MAS NMR and ^{29}Si MAS NMR respectively, with a Bruker Avance 500 spectrometer and the Si/Al ratio was investigated with the help of a Philips PU9200X atomic absorption spectrometer. Na$^+$ ions exchange process was observed by ^{23}Na MAS-NMR (Bruker Avance 500 spectrometer) and the generation of NH$_4^+$ ions was studied by FTIR with KBr pellets loaded with 1 wt.% of material, using a Perkin–Elmer Spectrum 2000 spectrometer.

2.3. Catalytic runs and analysis

To evaluate the performance of the catalysts for the high free fatty acid (FFA) oil esterification, palmitic acid was modified with 17% oleic acid. The esterification of palmitic acid with ethanol was performed in a 25 mL magnetically stirred round-bottomed flask fitted with a reflux condenser and an arrangement for digital temperature controller. The mixture of reaction was composed of a 60/1 ethanol/acid weight ratio and 0.6 wt.% catalyst was used. The reaction temperature was 130 °C and the stirring speed was 700 rpm. At the end of the experiment, the catalyst was separated from the reaction mixture by repeated centrifugation. The final acidity was measured by titration with 0.5 M sodium hydroxide solution. The conversion of FFA (x_{FFA}, in percents) was calculated by the acidity ratio using below formula:

$$x_{FFA} = \frac{a_s - a_t}{a_s} \times 100,$$

where a_s is the starting acidity of the reactant and a_t is the acidity at a "t" time. As reference, commercial Montmorillonite [Al$_2$O$_3$·4SiO$_2$·H$_2$O] clay purchased from Aldrich has been used.

Table 1
Names, pH conditions and textural properties of the synthesised and reference aluminosilicate materials.

Samples	pH	Al–Si ester/TMOS	S_{BET} (m^2/g)	V_p (cm^3/g)	Ø (nm)
Al–Si-13	13.0	–	361	0.5	5
Al–Si-13.5	13.5	–	219	0.4	5
Al–Si-TM13-1		1/1	315	0.6	5
Al–Si-TM13-2	13.0	2/1	326	0.6	5 and 10–20
Al–Si-TM13-4		4/1	289	0.4	<1.5 and 40–50
Al–Si-TM13.5-1		1/1	126	0.5	<1.5 and 5–15
Al–Si-TM13.5-2	13.5	2/1	72	0.5	<1.5 and 15–45
Al–Si-TM13.5-4		4/1	86	0.4	<1.5 and 15–45
Bentonite	–	–	62	<0.1	

3. Results and discussion

3.1. Morphological studies by scanning electron microscopy

The morphology of the materials prepared from the aqueous polymerisation of different Al–Si ester/TMOS ratios at pH of 13.0 and 13.5, was directly visualised by SEM (Fig. 1).

3.1.1. Effect of Al–Si ester/TMOS ratios at pH 13.0

The images, at different magnifications, of samples prepared with a 1/1 (Fig. 1a) and a 2/1 (Fig. 1b) molar ratio of Al–Si ester/TMOS, named Al–Si-TM13-1 and Al–Si-TM13-2 respectively (Table 1), display material only constituted of very large highly

spongy particles of ca. 60–80 μm which are comprised of very regular micrometer-sized spherically-shaped macrovoids. There are many of these 1–3 μm spherical voids, which are separated by thin walls and are found over the entire surface of the particle as well as within the particle. Fig. 1c shows the view at different magnification levels of the material prepared with an Al–Si ester/TMOS molar ratio of 4/1 (Al–Si-TM13-4) (Table 1). This material exhibits an irregular array of macrochannels.

These first results show that the introduction of TMOS as co-reactant is essential to generate the macroscaffold and the quantity of TMOS affects significantly the macrostructure. Indeed, when the alkoxysilane quantity is decreasing (from molar ratio of 1/1 to 4/1)
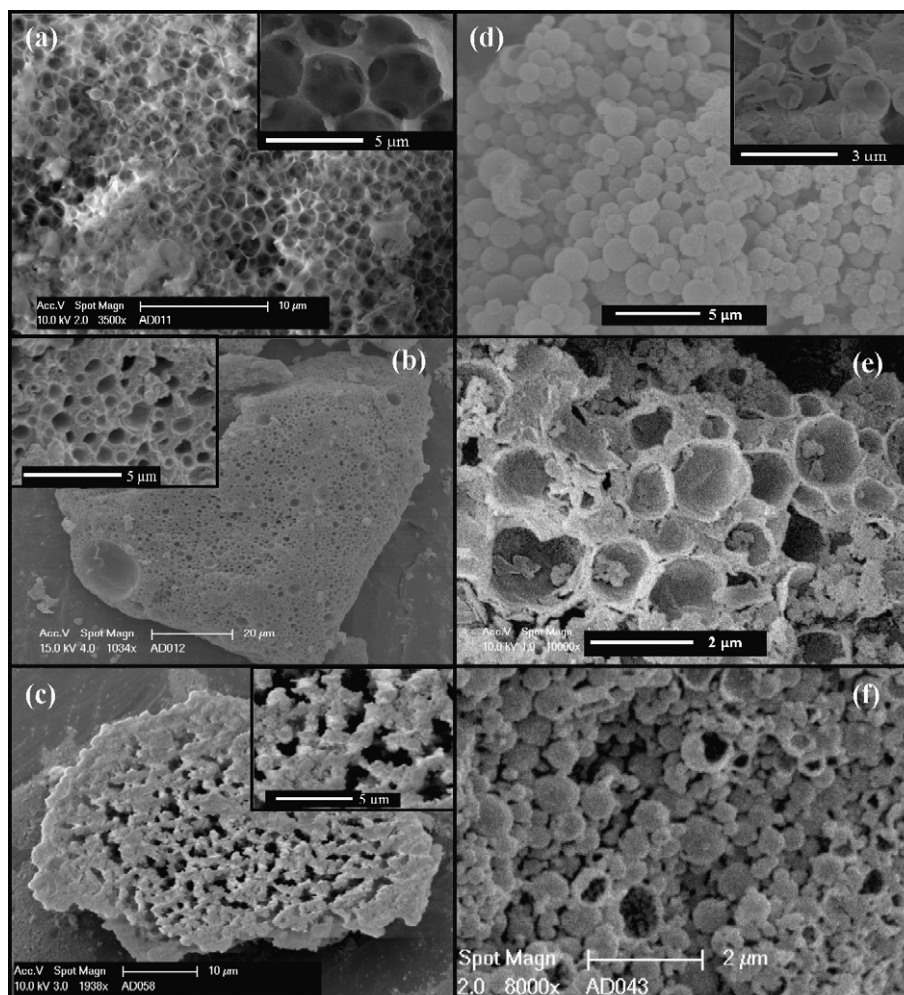
Fig. 1. SEM images of aluminosilicate particles synthesised at various ratio of Al–Si ester/TMOS at pH 13.0: (a) Al–Si-TM13-1, (b) Al–Si-TM13-2 and (c) Al–Si-TM13-4, and pH of 13.5: (d) Al–Si-TM13.5-1, (e) Al–Si-TM13.5-2 and (f) Al–Si-TM13.5-4.

or omitted entirely [64,69], the macroporosity evolves from a regular network of spherical cavities to a homogeneous arrangement of entangled macrochannels. Without adding TMOS, only few macroporous particles can be obtained [64,69]. When Al–Si-TM13-2 is compared to Al–Si-TM13-1, there is a lower proportion of macrovoids with decreased diameters. Al–Si-TM13-1 material exhibits interconnections between spherical voids due to the very thin walls separating each spherical cavity. Fig. 2A depicts the yield of meso-macroporous particles with different morphologies produced at different Al–Si ester/TMOS ratios at the pH of 13.0. It can be seen that with the increase in TMOS amount in the synthesis medium, the percentage or the yield of macroporous particles decreases, indicating that the introduction of more TMOS molecules reduces the production of macroporous particles and more TMOS molecules play the role to slow down the hydrolysis and condensation rates as expected, thus less breaking of Al–O–Si linkages.

3.1.2. Effect of Al–Si ester/TMOS ratios at pH 13.5

The slight increase in the pH value of the synthetic media induces a significant change in the morphology of particles. Fig. 1d–f represent SEM images at different magnification levels of Al–Si-TM13.5-1, Al–Si-TM13.5-2 and Al–Si-TM13.5-4 samples, and show that the macrostructure consists in the stacking of almost independent micro-sized (1–2 μm of diameter) hollow spheres. The impoverishment of TMOS in the initial mixture seems to not extensively affect the morphology. The abundance of macroporous particles, estimated by SEM investigations, is around 40%.
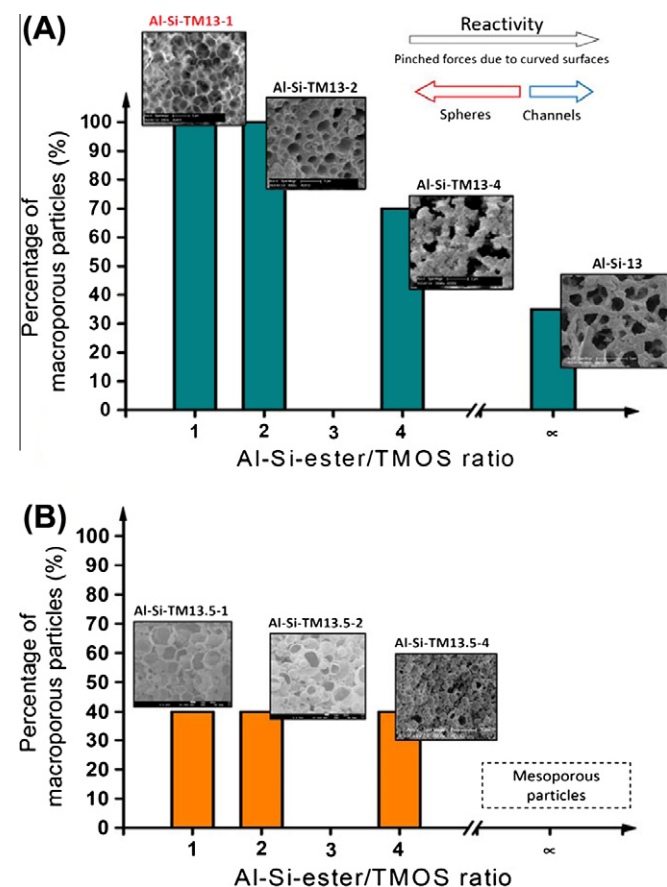
Fig. 2. Recapitulative schemes of the influence of the Al–Si-ester/TMOS ratio on the abundance and the morphology of the macroporosity at: (A) pH 13.0 and (B) at pH 13.5.

Fig. 1d, taken at higher resolution (pictures inserted), shows fully independent hollow spheres, among plausible debris of destroyed hollow bubbles. Obviously, increasing, even slightly, the pH value of the synthesis gel (whatever the amount of silica co-reactant) renders material spongier and more fragile. At this pH value, the effect of pH on the morphology predominates over the effect of Al–Si ester/TMOS molar ratios. Fig. 2B depicts the yield of meso-macroporous particles with different morphologies produced at different Al–Si ester/TMOS ratios at the pH of 13.5. It can be seen that at pH = 13.5, no significant change in the percentage or the yield of macroporous particles obtained is noted with the increase of TMOS amount. At this pH, Ph effect is more important than that of the amount of TMOS.

3.2. Textural properties by transmission electron microscopy

The presence of typical macrovoids is confirmed by TEM images of microtomed samples presented at Fig. 3.

3.2.1. Effect of Al–Si ester/TMOS ratios at pH 13.0

Fig. 3a displays TEM images at different magnification scales of the Al–Si-TM13-1 sample. TEM images highlight irregular openings of 1–3 μm large, surrounded by very thin walls of about 100–400 nm of thickness, and a deeper look into the macroporous skeleton reveals a vermicular mesoporosity (Fig. 3a and inset). Same observations are made for the sample Al–Si-TM13-2, albeit the mesoporous walls separating hollow spheres seem larger (about 200–800 nm long) and the regularity of the macrovoids is less noticeable (Fig. 3b and inset). As it is observed by SEM, the impoverishment of TMOS co-reactant reduces the size of the hollow spheres and enlarges mesoporous walls. TEM image (Fig. 3c) of the Al–Si-TM13-4 sample is also in agreement with the SEM observations (Fig. 1), indeed, only a disordered macrostructure constituted of very irregular openings is observed.

3.2.2. Effect of Al–Si ester/TMOS ratios at pH 13.5

The TEM image of Al–Si-TM13.5-1 sample (Fig. 3d) exposes a macroporous array which is comprised of spherical voids separated by even thinner walls. In certain areas, there is a great abundance of voids with connections arising between some of them. Macroporous material seems to be constructed by the stacking of independent and spherically shaped macrovoids of about 0.1–1 μm large, which is confirming SEM investigations (Fig. 1). High-magnification TEM image (Fig. 3d, inset) of the cross-sectional aluminosilicate Al–Si-TM13.5-1 specimen also reveals that these thin macroporous walls are composed of accessible disordered mesoporous arrays generated by the assembly of aluminosilicate nanoparticles of around 30 nm (Fig. 3d, inset), which could suggest an interparticular mesoporosity. Same observations are obtained about the Al–Si-TM13.5-2 sample in Fig. 3e. Only the mean size of the independent hollow spheres is somehow slightly reduced. TEM image at Fig. 3f of the Al–Si-TM13.5-4 material, exhibits a cross-section of these micro-sized hollow spheres and a deeper look shows that smaller hollow spheres of about 200 nm large, be difficultly visible on SEM images (Fig. 1), are also present. Again and interestingly, the reduction of TMOS amount in the starting mixture induces a visible diminution in the size of the hollow spheres.

3.3. Porosity by N$_2$ adsorption–desorption

All the nitrogen adsorption–desorption isotherms and corresponding pore size distribution of the samples synthesised at pH of 13.0 and 13.5 for various di-s-butoxyaluminoxytriethoxysilane
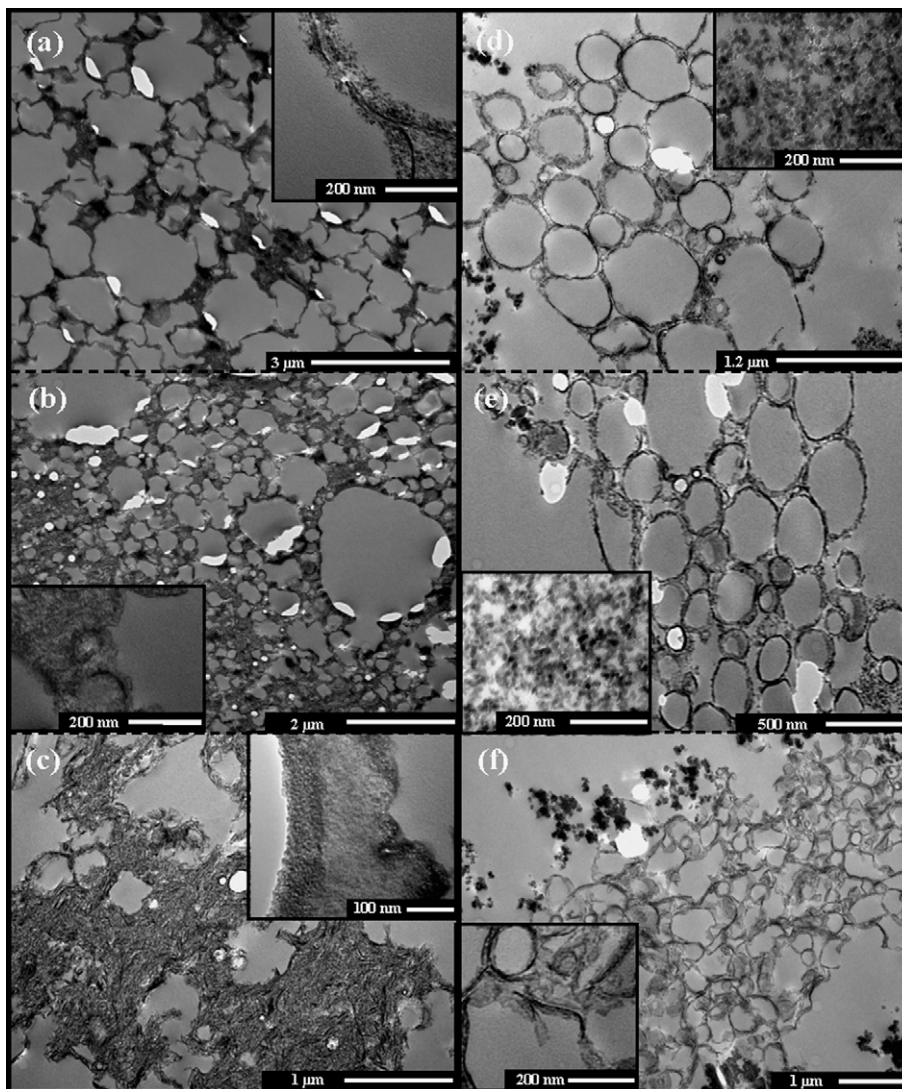
Fig. 3. Cross-sectional transmission electron microscopy (TEM) images of the aluminosilicate particles synthesised in the presence of varying amount of TMOS and presented in different magnifications at pH 13.0: (a) Al–Si–TM13-1, (b) Al–Si–TM13-2 and (c) Al–Si–TM13-4, and pH of 13.5: (d) Al–Si-TM13.5-1, (e) Al–Si-TM13.5-2 and (f) Al–Si-TM13.5-4.

and TMOS ratios are shown in Fig. 4. Textural properties such as accessible surface areas (S_{BET}), pore volumes (V_p) and pore sizes (Ø), are listed in Table 1.

3.3.1. Effect of Al–Si ester/TMOS ratios at pH 13.0

The isotherms of Al–Si-TM13-1 and Al–Si-TM13-2 samples, exhibited in Fig. 4a and b, belong to type IV, characteristic of mesoporous compounds. A capillary condensation step can be seen at relative pressures of around 0.75, indicating the presence of large pores. From these data sets, pore size distributions are calculated with maxima centred at $\sim$5 nm (Fig. 4a and b). The isotherm of Al–Si-TM13-2 sample display another step at high relative pressures ($p/p_0 \sim 0.8$) corresponding to a shoulder (black arrow) in the pore size distribution, located at $\sim$15 nm. Al–Si-TM13-1 and Al–Si-TM13-2 materials are characterised by high specific surface areas (see Table 1), which are 326 and 315 m^2/g respectively. In the case of Al–Si-TM13-4 material, (Fig. 4c), N$_2$ adsorption–desorption isotherms are the combination of both type I and II, which are typical of bimodal porous aluminosilicate materials. In the pore size distributions presented in Fig. 4c, the first maximum is centred in the super-microporous range (<2 nm). The second sharp steep

increase in N$_2$ adsorption is located at elevated relative pressure ($p/p_0 \geqslant 0.9$) corresponding to pore size distributions centred at a value higher than 40 nm. This last material possesses high specific surface area of 289 m^2/g. These BET analysis confirm the presence of a nanometer size scaled mesoporosity attested by TEM observations (Fig. 3c).

3.3.2. Effect of Al–Si ester/TMOS ratios at pH 13.5

Aluminosilicate materials synthesised in the more alkaline solution with TMOS present a combination of type I and type II isotherms (Fig. 4d–f). These isotherms are characteristic of supermicroporous structures with a pore size distribution inferior to 2 nm and also larger pores as it is shown by the sharp increase in N$_2$ adsorption located at very high relative pressure ($p/p_0 > 0.8$). This confirms again the presence of a secondary and larger porosity. The specific surface areas, reported in Table 1, for Al–Si-TM13.5-1, Al–Si-TM13.5-2 and Al–Si-TM13.5-4 are 126, 72 and 86 m^2/g respectively. The decrease in accessible surface area could arise from a slower rate of polymerisation at pH 13.5. The rapid assembly of aluminosilicate particles generates voids that correspond to the mesoporosity, which can be occluded if the
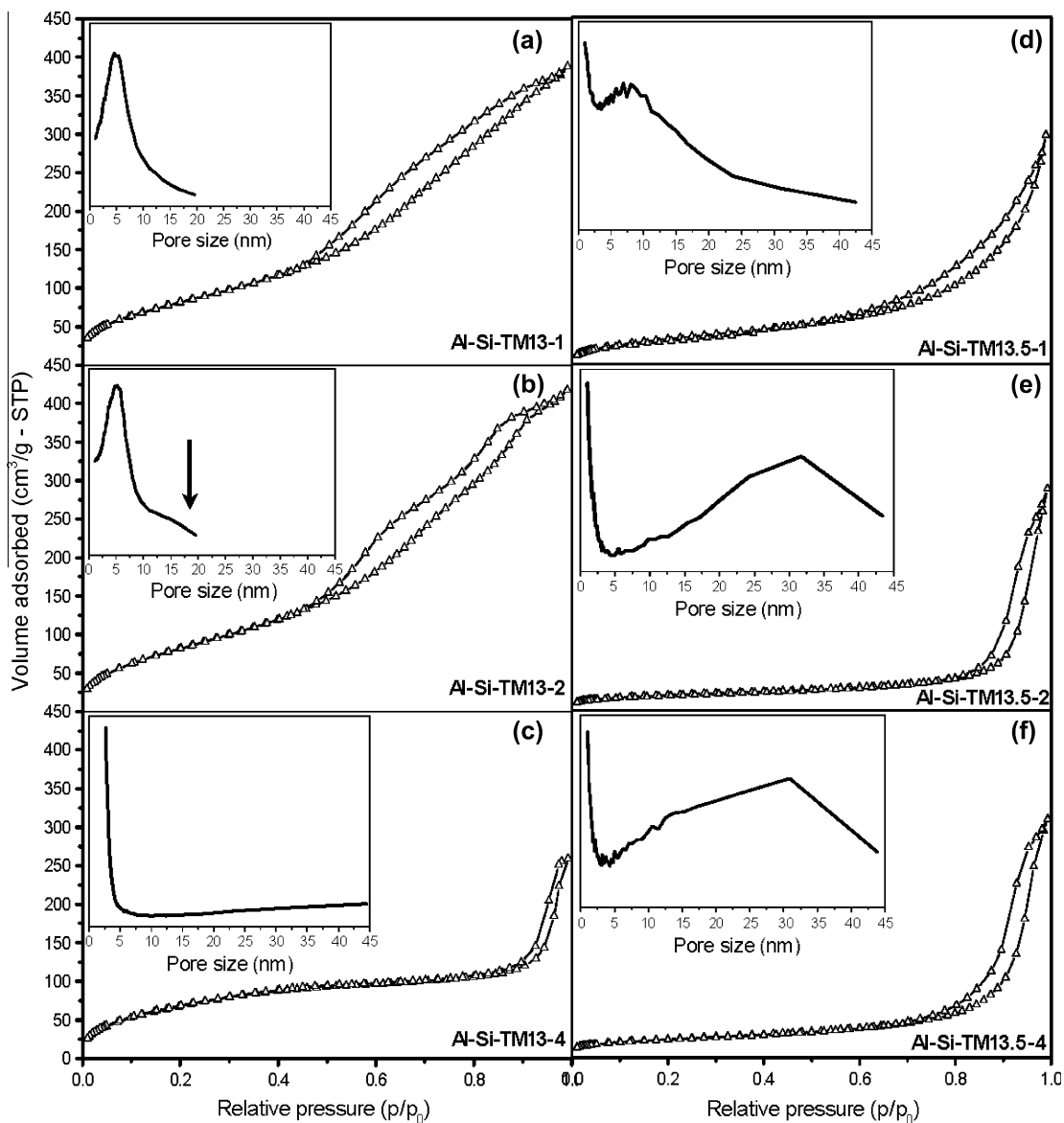
Fig. 4. N_2 adsorption–desorption isotherms and corresponding pore size distribution of the aluminosilicate samples prepared with varying Al–Si ester/TMOS at the pH of 13.0: (a) Al–Si–TM13-1, (b) Al–Si–TM13-2 and (c) TM13-4, and pH of 13.5: (d) Al–Si–TM13.5-1, (e) Al–Si–TM13.5-2 and (f) Al–Si–TM13.5-4.

nanoparticles can maximise their interactions during low aggregation processes. The second potential porosity corresponding to sharp increase in N_2 adsorption located at very high relative pressure could correspond to the interparticular porosity that is easily observed on TEM pictures at Fig. 3d–f. All the aluminosilicate samples investigated present pore volumes of around 0.5 cm^3/g. Except for the Al–Si-TM13-1 (Fig. 4a) sample, BET analysis coupled with BJH calculations exhibit that these materials show a fairly distinctive hierarchical biporosity (super-micro to large mesoporosity in most cases) in addition to a macroporous structure observed by TEM and SEM investigations. The large mesoporosity should arise from the self-aggregation of aluminosilicate particles and inside these nanoparticles, another super-micro- or mesoporosity could be generated during the release of solvents molecules.

3.4. Al and Si chemical environments and Si/Al ratios by solid state ^{27}Al and ^{29}Si MAS-NMR, and elemental analysis

The chemical activity of aluminosilicate materials is generally correlated to the presence of intra-framework aluminium atoms incorporated into the silica framework. The co-ordination environments of Al atoms in the samples were characterised by ^{27}Al MAS-NMR (Fig. 5). This method combined with elemental analysis (Table 2) yields the silicon to aluminium ratios (Si/Al) and silicon to tetrahedral aluminium ratio (Si/Al$_T$). All the ^{27}Al MAS-NMR spectra of the aluminosilicate materials exhibit a more intense peak at 55–60 ppm and another one around 0–6 ppm, corresponding respectively to tetrahedrally co-ordinated intra-framework aluminium species and octahedrally extra-framework aluminium species. The more intense peak at 55–60 ppm suggests that most of the aluminium atoms are located inside the inorganic porous framework on tetrahedral sites with the Si atoms, establishing Al–O–Si linkages.

As it was demonstrated previously [65,69], the addition of reactive silica co-reactant to the di-s-butoxyaluminoxytriethoxysilane single molecular precursor results in the elevation of the likelihood that heterocondensation reactions occur between an aluminium function and alkoxysilane site, producing Al–O–Si linkages instead of Al–O–Al bonds. Nevertheless, if the ratio of Al–Si ester/TMOS is too low, i.e. too high in the TMOS content, then a deficiency of
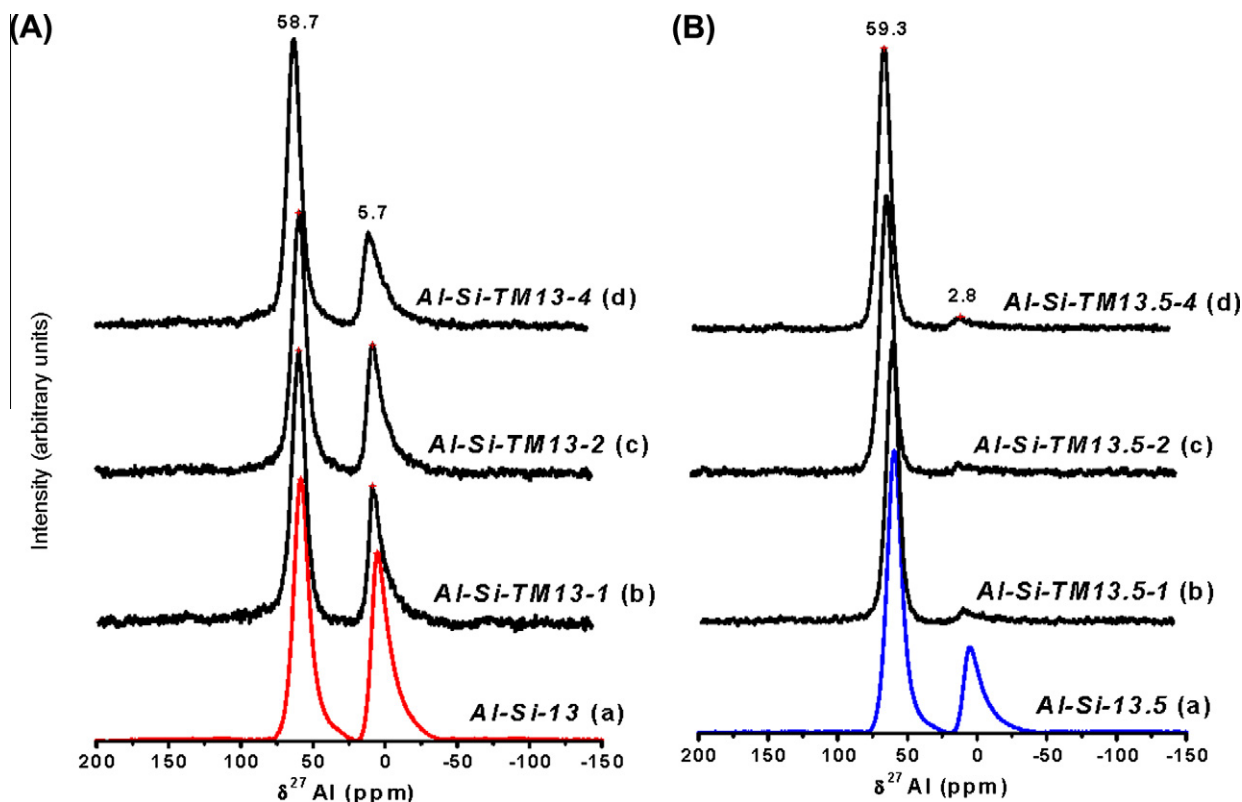
Fig. 5. ^{27}Al MAS-NMR spectra of aluminosilicate samples prepared with varying amount of TMOS at: (A) pH of 13.0: (a) Al–Si-13, (b) Al–Si-TM13-1, (c) Al–Si-TM13-2, (d) Al–Si-TM13-4, and (B) at pH of 13. (a) Al–Si-13.5, (b) Al–Si-TM13.5-1, (c) Al–Si-TM13.5-2, (d) Al–Si-TM13.5-4.

Table 2
Chemical compositions and Si/Al ratios of the presented aluminosilicate materials made by ^{27}Al and ^{29}Si MAS NMR and elemental analysis.

Samples	Si/Al	% Al_T	% Al_O	Si/Al_T
Al–Si-13	0.9	55	45	1.5
Al–Si-TM13-1	1.5	67	33	2.2
Al–Si-TM13-2	1.1	66	34	1.7
Al–Si-TM13-4	1.2	73	27	1.7
Al–Si-13.5	0.9	77	23	1.1
Al–Si-TM13.5-1	1.5	97	3	1.6
Al–Si-TM13.5-2	1.3	97	3	1.3
Al–Si-TM13.5-4	1.4	98	2	1.4
Bentonite	2			

aluminium within the meso-macroporous aluminosilicate material occurs, resulting in Si/Al and Si/Al_T ratios largely greater than the unity. It is observed that the incorporation of Al in tetrahedral position and the reduction of Al–O–Si linkage rupture are much more sensitive to the pH value of the media than to Al–Si ester/TMOS ratio. Hence elevated Al–Si ester/TMOS ratios were investigated with the maximal limitation fixed around 4/1 with respect to di-s-butoxyaluminoxytriethoxysilane, in order to conserve the pumice stone-like macroporous structure.

As can be seen in Fig. 5 and in Table 2, ^{27}Al MAS-NMR spectra of aluminosilicate materials synthesised at pH of 13.0 (Fig. 5A) and 13.5 (Fig. 5B) with the addition of increasing amount of TMOS exhibit an increase of the incorporation of aluminium into the silicated framework in comparison with aluminosilicate materials prepared without any co-reactant at pH of 13.0 (spectrum a Fig. 5A) or 13.5 (spectrum a of Fig. 5B). Addition of TMOS at pH of 13.0 (Fig. 5A), allows an increase of about 10% more of aluminium into the tetrahedral silicate framework in regard to Al–Si-13 material (Fig. 5Aa), independently to the Al–Si ester/TMOS ratios. The same trend is observed at pH 13.5, for which almost all the alu-

minium is tetrahedrally coordinated irrespective of the Al–Si ester/ TMOS ratios (Fig. 5B). This pH value yield materials only constituted of tetrahedral co-ordinated aluminium atoms, the resultant products are pure homogeneous aluminosilicate materials. Again, in comparison to the reference Al–Si-13.5 material (Fig. 5Ba) prepared without TMOS, a significant increase (more than 20%) of tetrahedral aluminium content is observed. Moreover, at pH 13.5, the lowest Si/Al and Si/Al_T ratios are obtained, even in the case of the richer silica co-reactant mixture (Table 2). The lowest Si/Al ratio ($Si/Al = Si/Al_T = 1.3$) is achieved with the meso-macroporous Al–Si-TM13.5-2 sample (Fig. 5Bc).

3.5. Mechanistic consideration of porous hierarchy formation

Previous works based on the optical microscopy suggested a macroporous architecture formation mechanism based on the polymerisation kinetics, i.e. the reactivity of the alkoxide precursors which determines the hydrodynamic flow of the hydrolysis and condensation by-product liquids (water and alcohol) released during fast polymerisation steps [49,64,65,69]. In other words, the macroporous structure can be formed only if the reactivity of alkoxide precursors is high enough to release very rapidly the water and alcohol by-product molecules which play the role of the porogen to generate the macrochannels. It was previously observed and also confirmed that when single or mixed metal alkoxides are used, parallel straight macrochannels crossing the whole the particle are obtained, whereas in the case of the intimate mixture of Al–Si ester/TMOS, interconnected spherically shaped macrocavities are produced. The present study showed that Al–Si ester/TMOS ratio and pH value can generate important differences regarding the macrostructure.

On the basis of Figs. 2A and 5A and at a pH of 13.0, the change in the Al–Si-ester/TMOS ratio did not modify significantly the
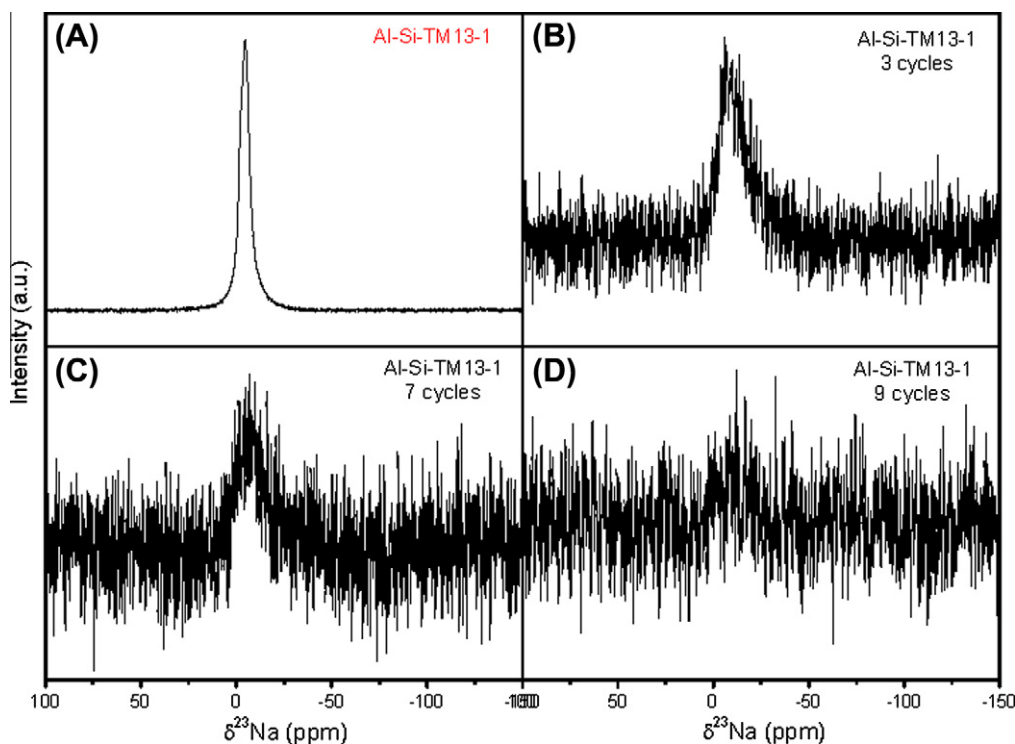
Fig. 6. ^{23}Na MAS-NMR spectrum of: (A) Al–Si-TM13-1 material after (B) 3, (C) 7 and (D) 9 ion exchange cycles.

incorporation of Al into the framework (Fig. 5A), whereas it induced an important modification in morphology (Fig. 2A). Al–Si ester/TMOS ratios upper than 4/1 are required to generate this pumice stone-like macroporous structure, higher amount of TMOS will slow down the polymerisation rate of the mixture of precursors to such a point that all the microsized liquid bubbles generated during the process should be expelled out the inorganic phase before being trapped due to its slow freezing rate. Decreasing the co-reactant amount, or without the additional silica precursor, the formation of a macroporous scaffold evolves due to higher polymerisation rates (but slower than polymerisation rate of usual metal alkoxide) of the less stabilized alkoxy-bridged single molecular precursors, inducing more pinched force due to importantly curved surfaces. The macrostructure morphology results into some intermediate situation between rectilinear macrochannels and regular spherically-shaped voids, a vermicular array of diameter-regular macrochannels [64].

For a pH of 13.5, no morphological (Fig. 2B), textural or chemical (Fig. 5B) modifications are recorded. Even for very low amount of TMOS (high Al–Si ester/TMOS), the morphology and abundance of the atypical macrostructure, constituted of micro-sized hollow mesoporous spheres, are preserved. This issue is certainly, in these extreme synthetic conditions, correlated to the dominant effect of the pH over the Al–Si ester/TMOS ratio on all the physico-chemical properties of this class of aluminosilicate materials.

3.6. Ion exchange study

Due to the synthesis of meso-macroporous aluminosilicates in alkaline media and due to the high amount of tetrahedral Al atoms incorporated in the silica framework, different negative charges were produced and are compensated by Na$^+$ ions present in the solution. ^{23}Na MAS-NMR and FTIR spectroscopy have been used to follow the Na$^+$ ions removal (Fig. 6) and the NH$_4^+$ generation processes (Fig. 7) respectively. This was illustrated with a sample synthesised from a mixture of single molecular precursor and TMOS at

pH = 13.0 (Al–Si-TM13-1). From Fig. 6, it is clearly observed that after synthesis, important amount of Na$^+$ ions are located at extra framework to compensate the negative charges of the rich Al tetravalent aluminosilicate framework. With increasing the cycle number of ion exchange, the intensity of the signal at around −5 ppm, assigned to Na$^+$ ions, decreased sharply, and disappeared completely after nine cycles of ion exchange (2% of residual Na$^+$ estimated by elemental analysis). Simultaneously, after 1 cycle of ion exchange, a peak located at 1429 cm^{-1} assigned to the bending vibration of H–N–H linkages of NH$_4^+$ ions [72] emerges (Fig. 7). The intensity of this peak increased with the increasing cycle number of ion exchange. All the above results showed the successful replacement of Na$^+$ ions by NH$_4^+$ ions. Fig. 8A and B respectively show that the relative amount of intra-framework aluminium species, as well as the form of N$_2$ adsorption–desorption isotherms
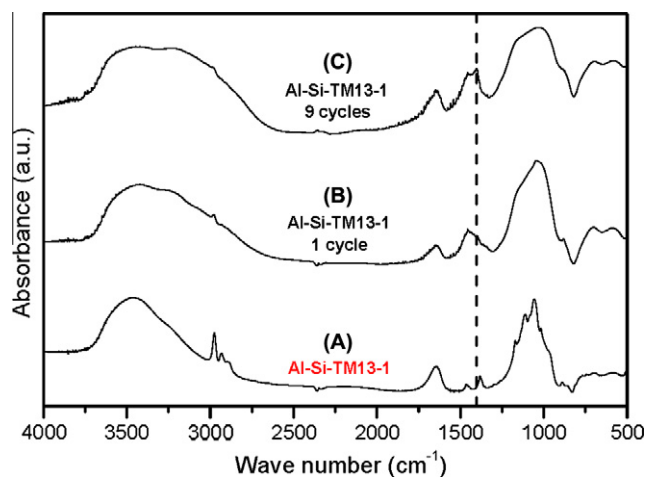
Fig. 7. FTIR spectrum of: (A) Al–Si-TM13-1 material after (B) 1 and (C) 9 ion exchange cycles.
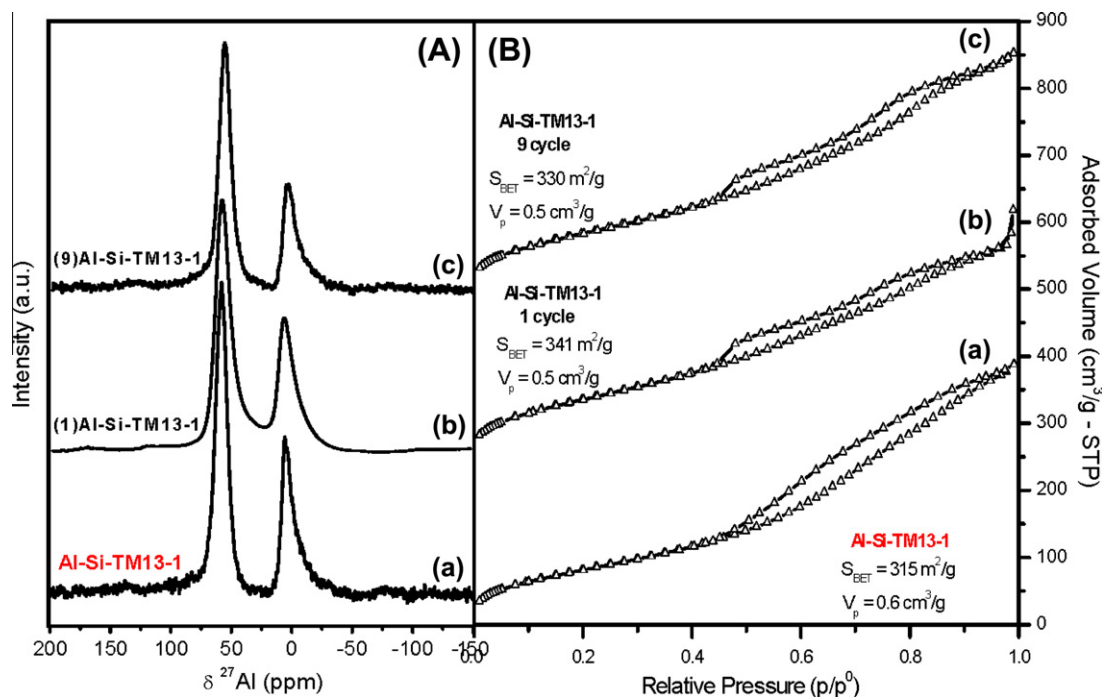
Fig. 8. (A) N_2 adsorption desorption isotherm of: (a) Al–Si-TM13-1 material after (b) 1 and (c) 9 ion exchange cycles and (B) ^{27}Al-MAS NRM spectra of: (a) Al–Si-TM13-1 material after (b) 1 and (c) 9 ion exchange cycles. The isotherms for (b) and (c) are offset by 200 and 400 cm^3/g, respectively, for clarity. Accessible surface areas determined by the BET method and porous volumes are symbolised by S_{BET} and V_p, respectively.

before and after ion exchange procedure remain unchanged. These observations are testifying that this process do not affect the properties of the aluminosilicate framework of the material.

3.7. Catalytic transesterification reactions

Fig. 9 exhibits the comparative conversion rate (in percents) of the palmitic/oleic acids mixture into esterified alkyl esters as a function of the reaction time for the Al–Si-TM13-1, Al–Si-TM13-2 and Al–Si-TM13-4 aluminosilicates, and for the commercial Bentonite clay. Slightly but evidently higher catalytic esterification conversions of fatty acids are, whatever the reaction time, globally observed for hierarchical meso-macroporous aluminosilicate materials. Al–Si-TM13-1, Al–Si-TM13-2 and Al–Si-TM13-4 samples are completely amorphous (XRD pattern not shown) and contain a
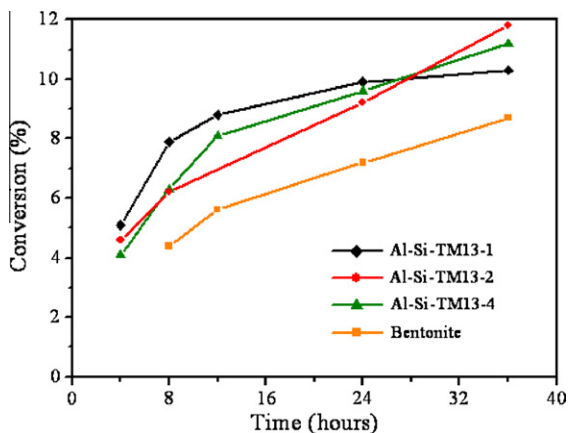
Fig. 9. Variation of the conversion percentage as a function of time for the esterification reaction of a palmitic/oleic mixture with ethanol, for different catalysts at 130 °C.

global Si/Al ratio of 1.1–1.5 and Si/Al$_T$ ratio of 1.7–2.2 (Table 2). The reference sample, Bentonite clay, contains a Si/Al ratio of 2. Our materials and the commercial reference clay have thus very close Si/Al ratios. The catalytic tests showed clearly, although the difference is limited, a better performance of synthesised meso-macroporous aluminosilicate materials. This is owing to the presence of meso-macroporosity in our samples, rendering a better accessibility of fatty acid molecules to catalytically active sites. In spite of their lower surface areas, catalytic conversion of palmitic/oleic acids mixture obtained with the materials prepared at a higher pH = 13.5 (Al–Si-TM13.5-1, Al–Si-TM13.5-2 and Al–Si-TM13.5-4 samples) are quite similar to the results observed with the material prepared at pH 13.0. This suggests that surface area of materials is not a predominant factor. Another important factor rendering our samples more active is their high tetrahedral Al content which gives a higher Bronsted acidity than Bentonite which contains mainly octahedral Al atoms. With their hierarchical meso-macroporosity and superior esterification activity of fatty acids, our samples, prepared from a single-source molecular precursor with TMOS as silica co-reactant via a self-formation strategy, will be a better FCC catalyst support to realise the pre-cracking procedure of large molecules, compared to a commercial clay used generally as FCC catalyst support. These new materials with hierarchical meso-macroporosity open new perspectives as catalysts or catalyst supports in a large series of acid catalysed reactions and as adsorbents in separation processes.

4. Conclusions

Hierarchically structured meso-macroporous aluminosilicates containing high content of tetrahedral aluminium featuring high number of active sites were successfully synthesised via the mixing of single-source molecular alkoxide precursor (sec-OBu)$_2$–Al–O–Si–(OEt)$_3$ and an inorganic silica co-reactant (TMOS). By the modification of the (sec-OBu)$_2$–Al–O–Si–(OEt)$_3$/alkoxysilane molar ratios ranging to 1/1–4/1, this strategy leads to the design of a new

generation of stabilized alkoxy-bridged single molecular precursors with modified aqueous reactivities. This results in a significant increased amount of tetrahedral aluminium atoms incorporated into the aluminosilicate framework. In the case of strongly alkaline solutions (pH around 13.5), quite pure aluminosilicate materials, only constituted of intra-framework aluminium species, are produced. The modification of the precursors reactivity also produces a self-generated 3D spherically-shaped (interconnected spherical cavities at pH of 13.0 and independent hollow spheres at pH of 13.5) macroporous scaffold by the release of large amount of liquid hydrolysis and condensation by-products acting as a porogen. These macropores are separated by very thin wormhole-like mesoporous walls. A greater quantity of TMOS, above a 1/1 ratio, is resulting in higher Si/Al ratios and the disappearance of the macroporous structure. However smaller amounts do not favour hetero-condensation between the extremely hydrolytic aluminium functional groups and the siloxane functional groups (octahedral aluminium species are more prevalent). Additionally, decreasing TMOS content in the starting mixture modifies the macrostructure morphology toward a vermicular network of regular macrochannels, due to the concomitant generation of numerous curved surfaces and additional pinched force applied on the liquid hydrolysis and condensation by-product porogen microbubbles. Ion exchange was successfully achieved without any degradation of textural, morphological or structural properties. Newly generated acid-type aluminosilicate materials were then used in transesterification reactions of a FFA mixture with ethanol, and compared with a commercial aluminosilicate Montmorillonite clay support with similar Si/Al ratio, used in catalytic processes. Newly synthesised acid materials present slightly but clearly evident higher esterification conversion rates, owing to the hierarchical meso-macrostructure. These easily synthesised meso-macroporous aluminosilicate materials appear to be promising candidates for supporting catalysts in vital industrial processes.

Acknowledgments

References

[1] H. Maekawa, J. Esquena, S. Bishop, C. Solans, B.F. Chmelka, Adv. Mater. 15 (2003) 591.
[2] H.R. Chen, J.L. Gu, J.L. Shi, Adv. Mater. 17 (2005) 2005.
[3] P. Yang, T. Deng, D. Zhao, P. Feng, D. Pine, B.F. Chmelka, G.M. Whitesides, G.D. Stucky, Science 282 (1998) 2244.
[4] S. Pega, C. Boissière, D. Grosso, T. Azaïs, A. Chaumonnot, C. Sanchez, Angew. Chem. Int. Ed. 48 (2009) 2784.
[5] F. Carn, N. Steunou, J. Livage, R. Backov, Chem. Mater. 17 (2005) 644.
[6] D.T. On, S. Kaliaguine, Angew. Chem. Int. Ed. 40 (2001) 3248.
[7] D.T. On, S. Kaliaguine, Angew. Chem. Int. Ed. 41 (2002) 1036.
[8] R.A. Caruso, M. Antonietti, Adv. Funct. Mater. 12 (2002) 307.
[9] V. Valtchev, M. Smaihi, A.C. Faust, L. Vidal, Angew. Chem. Int. Ed. 42 (2003) 2782.
[10] X. Chen, X. Wang, X. Fu, Energy Environ. Sci. 2 (2009) 872.
[11] X.Y. Yang, Y. Li, A. Lemaire, J.G. Yu, B.L. Su, Pure Appl. Chem. 81 (2009) 2265.
[12] A. Corma, Chem. Rev. 97 (1997) 2373.
[13] A. Corma, H. Garcia, Chem. Rev. 102 (2002) 3837.
[14] E.G. Judith, J. Wijnhoven, W.L. Vos, Science 281 (1997) 802.
[15] B.T. Holland, C.F. Blanford, A. Stein, Science 281 (1998) 538.
[16] P. Jiang, J.F. Bertone, V.L. Colvin, Science 291 (2001) 453.
[17] D. Walsh, L. Arcelli, T. Ikoma, J. Tanaka, S. Mann, Nat. Mater. 2 (2003) 386.
[18] F. Carn, A. Colin, M.-F. Achard, H. Deleuze, Z. Saadi, R. Backov, Adv. Mater. 16 (2004) 140.
[19] G.T. Chandrappa, N. Steunou, J. Livage, Nature 416 (2002) 702.
[20] A. Imhof, D.J. Pine, Nature 389 (1997) 948.
[21] A. Imhof, D.J. Pine, Adv. Mater. 10 (1998) 697.
[22] H. Nishihara, S.R. Mukai, D. Yamashita, H. Tamon, Chem. Mater. 17 (2005) 683.
[23] Z.Y. Yuan, B.L. Su, J. Mater. Chem. 16 (2006) 663.
[24] S.A. Davis, S.L. Burkett, N.H. Mendelson, S. Mann, Nature 385 (1997) 420.
[25] B.T. Holland, L. Abrams, A. Stein, J. Am. Chem. Soc. 121 (1999) 4308.
[26] L. Huang, Z. Wang, J. Sun, L. Miao, Q. Li, Y. Yan, D. Zhao, J. Am. Chem. Soc. 122 (2000) 3530.
[27] B. Zhang, S.A. Davis, N.H. Mendelsonb, S. Mann, Chem. Commun. 9 (2000) 781.
[28] V. Valtchev, M. Smaihi, A.C. Faust, L. Vidal, Angew. Chem. Int. Ed. 42 (2003) 2782.
[29] Z.Y. Yuan, J.L. Blin, B.L. Su, Chem. Commun. 5 (2002) 504.
[30] A. Léonard, B.L. Su, Colloids Surf. A: Physicochem. Eng. Aspects 300 (2007) 129.
[31] A. Vantomme, A. Léonard, Z.Y. Yuan, B.L. Su, Colloids Surf. A: Physicochem. Eng. Aspects 300 (2007) 70.
[32] P.Y. Dapsens, S.H. Hakim, B.L. Su, B.H. Shanks, Chem. Commun. 46 (2010) 8980.
[33] W. Deng, M.W. Toepke, B.H. Shanks, Adv. Funct. Mater. 13 (2003) 61.
[34] A. Collins, D. Carriazo, S.A. Davis, S. Mann, Chem. Commun. 5 (2004) 568.
[35] T.Z. Ren, Z.Y. Yuan, B.L. Su, Chem. Commun. 23 (2004) 2730.
[36] W. Deng, B.H. Shanks, Chem. Mater. 17 (2005) 3092.
[37] S.H. Hakim, B.H. Shanks, Chem. Mater. 21 (2009) 2027.
[38] Z.Y. Yuan, T.Z. Ren, A. Vantomme, Chem. Mater. 16 (2004) 5096.
[39] B.L. Su, A. Vantomme, L. Surahy, R. Pirard, J.P. Pirard, Chem. Mater. 19 (2007) 3325.
[40] X.Y. Yang, Y. Li, G. Van Tendeloo, F.S. Xiao, B.L. Su, Adv. Mater. 21 (2009) 1368.
[41] Z.Y. Yuan, T.Z. Ren, A. Azioune, J.J. Pireaux, B.L. Su, Chem. Mater. 18 (2006) 1753.
[42] T.Z. Ren, Z.Y. Yuan, B.L. Su, Langmuir 20 (2004) 1531.
[43] J.L. Blin, A. Léonard, Z.Y. Yuan, L. Gigot, A. Vantomme, A.K. Cheetam, B.L. Su, Angew. Chem. Int. Ed. 42 (2003) 2872.
[44] A. Vantomme, Z.Y. Yuan, B.L. Su, New J. Chem. 28 (2004) 1083.
[45] Z.Y. Yuan, A. Vantomme, A. Léonard, B.L. Su, Chem. Commun. 13 (2003) 61.
[46] Z.Y. Yuan, T.Z. Ren, B.L. Su, Adv. Mater. 15 (2003) 1462.
[47] T.Z. Ren, Z.Y. Yuan, B.L. Su, Chem. Phys. Lett. 388 (2004) 46.
[48] Z.Y. Yuan, T.Z. Ren, A. Azioune, J.J. Pireaux, B.L. Su, Catal. Today 105 (2005) 647.
[49] Y. Li, X.Y. Yang, G. Tian, A. Vantomme, J.G. Yu, G. Van Tendeloo, B.L. Su, Chem. Mater. 22 (2010) 325.
[50] A. Corma, M.E. Domine, L. Nemeth, S. Valencia, J. Am. Chem. Soc. 124 (2002) 3194.
[51] G.J. de A.A. Soler Illia, C. Sanchez, Lebeau B. Patarin, J. Chem. Rev. 102 (2002) 4093.
[52] M.T. Janicke, C.C. Landry, S.C. Christiansen, S. Birtalan, G.D. Stucky, B.F. Chmelka, Chem. Mater. 11 (1999) 1342.
[53] A. Léonard, J.L. Blin, B.L. Su, Chem. Commun. 14 (2003) 2568.
[54] A. Léonard, B.L. Su, Chem. Commun. 14 (2004) 1674.
[55] X.Y. Yang, A. Léonard, A. Lemaire, G. Tian, B.L. Su, Chem. Commun. 10 (2011) 2763.
[56] K.W. Terry, T.D. Tilley, Chem. Mater. 3 (1991) 1001.
[57] K.W. Terry, P.K. Ganzel, T.D. Tilley, Chem. Mater. 4 (1992) 1290.
[58] K.W. Terry, P.K. Ganzel, T.D. Tilley, Inorg. Chem. 32 (1993) 5402.
[59] K.L. Fujdala, T.D. Tilley, J. Catal. 216 (2003) 265.
[60] X.Y. Yang, A. Vantomme, A. Lemaire, F.S. Xiao, B.L. Su, Adv. Mater. 18 (2006) 2117.
[61] X.Y. Yang, A. Vantomme, F.S. Xiao, B.L. Su, Catal. Today 128 (2007) 123.
[62] A.D. Irwin, J.S. Holmgren, J. Jonas, J. Mater. Sci. 23 (1988) 2908.
[63] J.B. Miller, E.R. Tabone, E.I. Ko, Langmuir 12 (1996) 2878.
[64] A. Lemaire, B.L. Su, Langmuir 26 (2010) 17603.
[65] A. Lemaire, B.L. Su, Microporous Mesoporous Mater. 1 (2011) 70.
[66] T.W. Swaddle, J. Salerno, P.A. Tregloan, Chem. Soc. Rev. 23 (1994) 319.
[67] T.W. Swaddle, Coord. Chem. Rev. 219 & 221 (2001) 665.
[68] C.J. Brinker, G.W. Scherer, Sol–Gel Science, The Physics and Chemistry of Sol–Gel Processing, San Diego, 1999.
[69] A. Lemaire, J.C. Rooke, L.H. Chen, Langmuir 27 (6) (2011) 3030.
[70] A.C. Carmo Jr., L.K.C. de Souza, C.E.F. da Costa, E. Longo, J.R. Zamian, G.N. da Rocha Filho, Fuel 88 (2009) 461.
[71] K.H. Chung, D.R. Chang, B.G. Park, Bioresour. Technol. 99 (2008) 7438.
[72] B.L. Su, V. Norberg, Zeolites 19 (1997) 65.